

Design and Analysis of Non-Conventional Dielectric Dome Antenna for Scan Enhancement

Amrit Raj
Dept. of ECE
RV College of Engineering
Bangalore, India
amritraj.ec21@ieee.org

Madhusudhan T M
Dept. of ECE
RV College of Engineering
Bangalore, India
madhusudhantm@ieee.org

Mahesh A
Dept. of ECE
RV College of Engineering
Bangalore, India
mahesha@ieee.org

Ashutosh Kedar
Scientist F
LRDE, DRDO
Bangalore, India
ashutosh.kedar@ieee.org

Abstract—This paper investigates the design and performance of non-conventional dielectric dome antennas integrated with a 4x4 Microstrip Patch Antenna Array (MPAA). The primary objective is to enhance the wide-angle scanning capabilities of the antenna for modern communication and radar systems. Three distinct dome designs were analyzed: Design 1 and Design 2 prioritizing the maximization of scanning range, and Design 3 focusing on minimizing dome size and gain drop at boresight angles. The results indicate substantial improvements in beam shaping and scanning capabilities with the incorporation of dielectric domes. While the scanning ability of MPAA is limited to 45 degrees, all three dome designs significantly enhanced the scanning range and maintained acceptable gain levels. Notably, Design 2 achieved a Scanning range of upto 70 degrees and Design 3 showed 1 dB increase in boresight gain compared to other two domes.

Index Terms—Keywords—Dielectric dome, Microstrip Patch Antenna Array, Beam Scanning, Acrylonitrile Butadiene Styrene

I. INTRODUCTION

The telecommunications and Radio Frequency (RF) industries are advancing towards sophisticated wireless and sensing technologies. These advancements require more capable antenna systems. Notably, MPAAAs are evolving due to their high performance, low cost, and easy integration [1]. Electronically steerable arrays are preferred for beam scanning in satellite communication (SATCOM), automotive radar, and military/defense technologies [2]. Nearly hemispherical scanning is crucial for applications such as SATCOM mobile terminals, base stations, and radars. While mechanically scanned antennas offer this capability, they are bulky and unsuitable for stringent volume requirements, especially in airborne solutions where low drag and weight are critical. Thus, fully electronic beam-steering is preferable.

Non-conventional dielectric domes integrated with MPAAAs offer a solution, optimizing shape and thickness to maintain high gain across broad angles, overcoming limitations of traditional arrays. Rotational dielectric domes with linear array feeds achieve uniform high gain over wide angles [3]. Designs using dielectric domes enhance beam scanning and gain, outperforming traditional arrays [4]. Comparative studies show multi-layered and solid lens structures significantly improve gain but with limited scanning range [5]. Experimental results show that dielectric domes achieve reduced profiles with wide scanning capability, proving their practical applicability [6].

Phase-gradient meta-domes increase grating-lobe-free scan ranges, balancing gain and scan performance [7]. Ray tracing studies refine lens design, enhancing efficiency and performance [8], [9]. Fully metallic geodesic Luneburg lenses show potential for compact, high-performance multibeam systems [10].

In this paper, Three different non-conventional dielectric domes made of Acrylonitrile Butadiene Styrene (ABS) material with a dielectric constant of $D_k = 3$ and a loss tangent of $\tan \delta = 0.012$ are studied. Unlike prior works that focus on single performance metrics, this study balances multiple aspects, such as maximizing scanning range (Design 1 and Design 2) and minimizing dome size while reducing gain drop at boresight (Design 3). This multi-objective optimization is a novel approach that addresses practical constraints in antenna design. The primary feed element for the dielectric dome is a 4x4 MPAA with an RT Duroid 5880 substrate, which has notable performance in the C-band. Section II describes the design and simulation of three types of non-conventional dielectric domes, Section III describes Ray tracing analysis. Section IV discusses the results for all three cases considered, and Section V summarizes the work.

II. DESIGN OF DIELECTRIC DOMES

In this study, three types of dielectric dome lenses are considered: Design 1, Design 2, and Design 3, as shown in Fig. 1(a) - (c). All the domes are rotationally symmetric around their central axis and are illuminated by a 4x4 MPAA. The array is designed to operate at 5.65 GHz. The element periodicity is $\lambda/2 = 2.65$ cm and the dimension of a single patch is 1.550 x 1.635 cm. The 4x4 MPAA has a dimension of 11.24 x 11.24 cm as shown in Fig. 2. 'L' in Fig. 1 refers to the length of patch array. The dielectric dome is characterized by its dielectric constant D_k , and its inner and outer surface shapes, s_1 and s_2 respectively. Designs 1 and 2 are optimized for wide scanning, while Design 3 is optimized to minimize the dome size and gain drop at boresight, Compromising with the scanning range of the antenna.

A. Dome Design 1

The non-conventional dome of Design 1, is illustrated in Fig. 1(a). The diameter of the inner surface (s_1) of dome is designed as twice the length of 4x4 MPAA. To calculate the

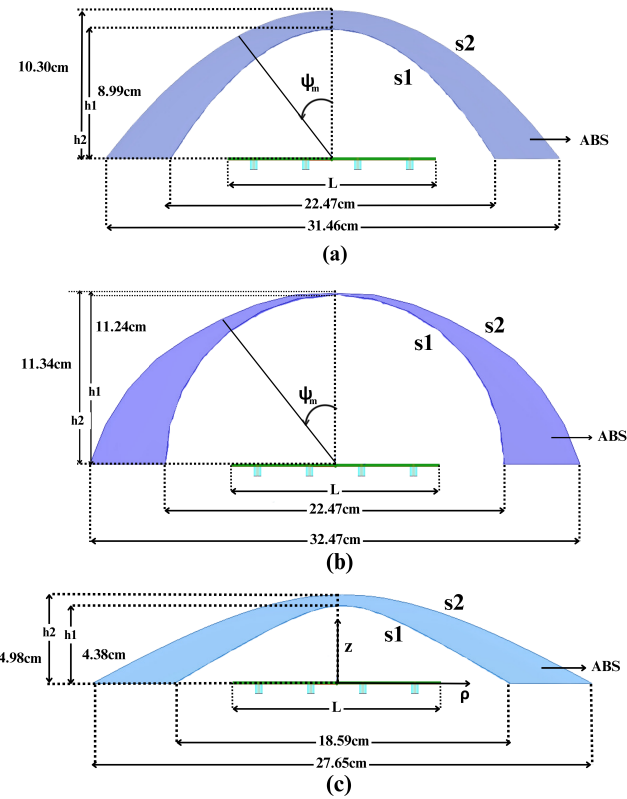


Fig. 1. (a) Design 1 with 4x4 MPAA (b) Design 2 with 4x4 MPAA (c) Design 3 with 4x4 MPAA.

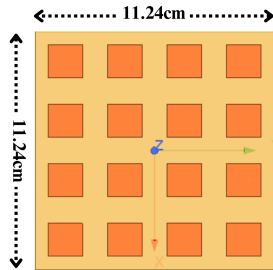


Fig. 2. Structure of 4x4 MPAA.

height of the inner surface, the ratio C as shown in (1) is used where $C = 0.3$ cm and $L = 11.24$ cm resulting in height of inner surface $h_1 = 8.99$ cm. For determining the diameter of the outer surface, (2) obtained from [3] is applied. The term $r_{m,0}(\psi)$ is the initial radius of the dome before any variations. The second term, which involves a sum of products of coefficients $a_{m,i}$ and functions $g_m^i(\psi)$, varies the outer surface radius to optimize its performance. The outer dome surface s_2 is calculated by varying the angle ψ_m from 0° to 90° (top to bottom) along the perimeter. The function $g_m^i(\psi)$ shown in (3) defines the modification applied to the initial shape $r_{m,0}(\psi)$ based on the angle ψ [3]. If ψ is less than a certain threshold angle ψ_m , the function is zero, meaning no variation is made. For ψ greater

than or equal to ψ_m , the variation is applied according to the polynomial $\left(\frac{\psi - \psi_m}{\Psi}\right)^i$, where Ψ is a scaling constant and i is the order of the polynomial term which is taken as 1 due to a single layered structure of dome. Based on the 4x4 MPAA profile, the dimensions of the outer dome are optimised by considering $a_{m,i} = 5$, for the thickness of the structure to be 5 cm at $\psi_m = 90^\circ$ [3]. To calculate $g_m^i(\psi)$, the values of ψ_m and Ψ are taken as 30° and 60° , respectively, with ψ_m varying between 0° and 90° . By using curve-fitting algorithm points obtained from (3) are interpolated and the surfaces are plotted. Ray tracing analysis is performed on the obtained surfaces to analyse how the rays interact with the dome surfaces.

$$C = \frac{h_1}{2L} \quad (1)$$

$$r_m(\psi) = r_{m,0}(\psi) + \sum_{i=1}^K a_{m,i} g_m^i(\psi) \quad (2)$$

$$g_m^i(\psi) = \begin{cases} 0 & \psi < \psi_m \\ \left(\frac{\psi - \psi_m}{\Psi}\right)^i & \psi \geq \psi_m \end{cases} \quad (3)$$

B. Dome Design 2

Dome Design 2 is depicted in Fig. 1(b). The diameter of inner surface s_1 is considered to be twice the length of 4x4 MPAA. To calculate the height of the inner surface h_1 , the ratio $C = 0.5$ and length $L = 11.24$ cm, is used as indicated in (1), The resulting value of h_1 is 11.24 cm. the dimensions of the outer dome surface is calculated by using (2) and (3).

C. Dome Design 3

In the previous two designs (Design 1 and Design 2), the dimensions of the dome is not considered as a design constraint. However, in this design, the focus is on minimizing the size of the dome to meet the requirements for applications where the form factor is critical. A lower boundary for the height of the dome is obtained from [6] which is approximately 0.35 times the length of array (L). The surfaces of Dome 3 are described by the conic equation (4), obtained from [6].

$$z = h_i + \frac{c_l \rho^2}{1 + \sqrt{1 - (1 + K_i)c_l^2 \rho^2}} \quad (4)$$

In this equation, h_i , c_i , and K_i represent the height, curvature, and conic constant, respectively, while ρ denotes the radial coordinate in the plane of the array. The subscript $i = 1, 2$ refers to the internal (s_1) and external (s_2) surfaces as shown in Fig. 1 (c). The variables h_2 , c_1 , c_2 , K_1 , and K_2 are optimized to enhance the scanning performance. Meanwhile, the height of the internal surface h_1 is determined based on the size constraints of the dome. In this design the height of the inner surface h_1 is fixed at 4.38 cm and other parameters were optimized to maximize the area illuminated by the array for the largest scanning angle of 60° using the ray tracing analysis. The optimized parameters of the dome are given in Table I

TABLE I
OPTIMIZED PARAMETERS OF DESIGN 3

Surface	c_i (m^{-1})	K_i	h_i (cm)
s_1	-24	-3.7	4.38
s_2	-7.4	-3.4	4.98

III. RAY-TRACING ANALYSIS

Ray tracing is a fundamental technique used to analyze the performance of dielectric domes. This method allows for the visualization of how electromagnetic waves propagate through different dome designs, helping to identify the optimal configurations for beam shaping and wide-angle scanning. In this study, inverse ray tracing was employed to evaluate the scanning performance of dielectric dome designs at boresight and extreme scan angles. Fig. 3 shows the ray tracing results of all dome designs at boresight and extreme scan angles. At boresight, the rays maintained a coherent pattern and At extreme scan angles the rays began to diverge slightly, indicating the start of beam spread.

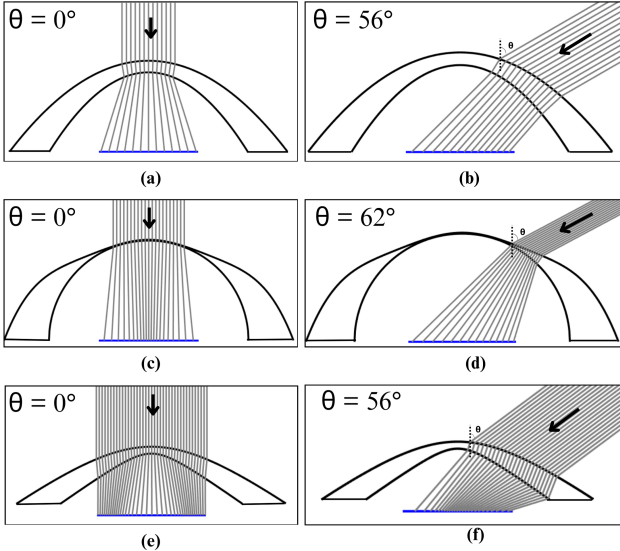


Fig. 3. Inverse Ray-tracing results for $\Phi = 0^\circ$ plane. Design 1:(a) Ray-tracing for boresight and (b) for $\theta = 56^\circ$ scanning. Design 2: (c) Ray-tracing for boresight and (d) for $\theta = 62^\circ$ scanning. Design 3 (e) Ray-tracing for boresight and (f) for $\theta = 56^\circ$ scanning

IV. RESULTS AND DISCUSSIONS

The simulation results for the 4x4 MPAA with various dome designs are discussed in this section. The primary radiator is restricted to 4x4 due to limited simulation resources available. The dome structures are designed in SolidWorks using the profile obtained from ray tracing, and the simulation and optimization of the dielectric dome antenna are carried out using Ansys HFSS. The return loss of the 4x4 MPAA array integrated with 3 designs of the dielectric dome are shown in Fig. 4. The standalone 4x4 MPAA has a return loss of -27.56 dB. The best return loss is observed with Design 2, which

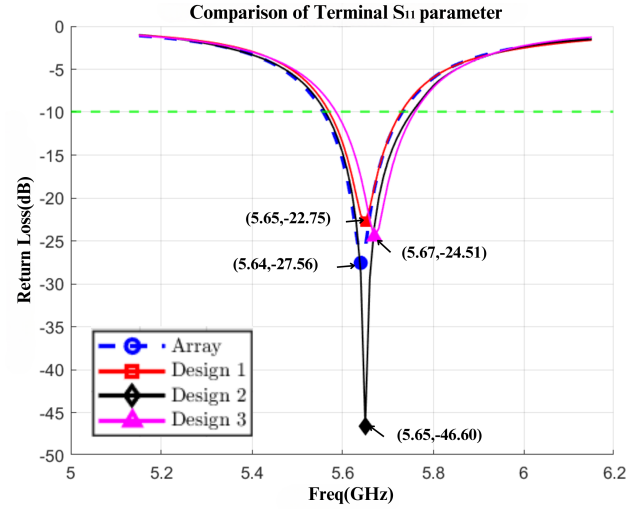


Fig. 4. Return Loss of 4x4 MPAA with and without dielectric domes.

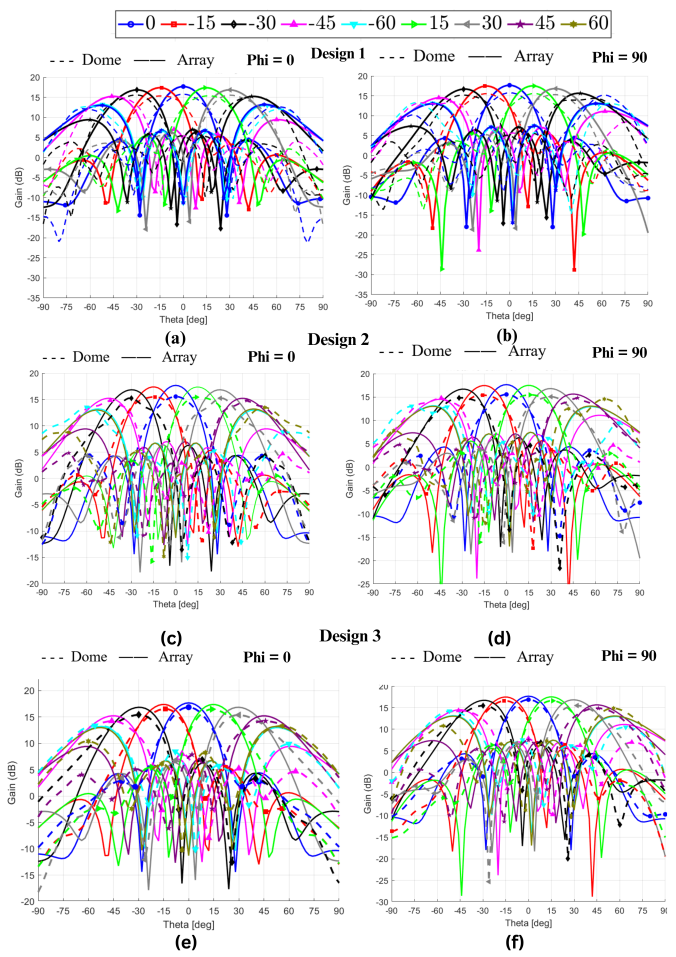


Fig. 5. Beam steering results of 4x4 MPAA for different values of θ with, (a) Design 1 at $\Phi = 0^\circ$ (b) Design 1 at $\Phi = 90^\circ$ (c) Design 2 at $\Phi = 0^\circ$ (d) Design 2 at $\Phi = 90^\circ$ (e) Design 3 at $\Phi = 0^\circ$ (f) Design 3 at $\Phi = 90^\circ$.

TABLE II
BEAM STEERING RESULT COMPARISON

Structure	4x4 MPAA			Design 1		
Plane	Scanning Angle θ (degrees)	Gain [dBi]	PSLL [dBi]	Scanning Angle θ (degrees)	Gain [dBi]	PSLL [dBi]
$\Phi = 0^\circ$	0	17.63	4.35	0	15.77	4.15
	45	15.19	6.98	56	13.99	6.75
$\Phi = 90^\circ$	0	17.63	3.54	0	15.77	4.20
	45	15.64	7.15	62	14.94	7.40
Structure	Design 2			Design 3		
Plane	Scanning Angle θ (degrees)	Gain [dBi]	PSLL [dBi]	Scanning Angle θ (degrees)	Gain [dBi]	PSLL [dBi]
$\Phi = 0^\circ$	0	15.56	4.35	0	16.87	2.82
	62	12.81	5.22	56	13.87	8.23
$\Phi = 90^\circ$	0	15.59	3.54	0	16.87	3.16
	70	14.78	7.45	58	14.87	7.28

is -46.60 dB, showing better performance than the standalone array. Designs 1 and 3 have return losses of -22.75 dB and -24.51 dB, respectively, which are comparable with the array.

The co-polar radiation patterns of the 4x4 MPAA with various dome designs for different values of θ in $\Phi = 0^\circ$ and $\Phi = 90^\circ$ plane at the central frequency are reported in Fig. 5(a) - 5(f). Table II presents the beam steering results for boresight and maximum scan angle. The distance between dome and the primary radiator is optimized for better gain at the boresight and extreme angles. Design 1 and 2 are at the same level with primary radiator and Design 3 is at 1 cm above the primary radiator. Results show that at a scanning angle of 0° , the peak gain of the array without the dome is 17.63 dBi, while with the integration of the dome, the gain is reduced by approximately 2 dB for Design 1 and 2 and by 1 dB for Design 3 at the boresight. This is due to the curvature of the dielectric dome. The standalone 4x4 MPAA exhibits scanning upto $\pm 45^\circ$ but with the integration of the lens, the performance is significantly improved for wide scanning in all the cases. Design 1 can radiate the beam to a maximum scan angle of $\pm 56^\circ$ at $\Phi = 0^\circ$ and $\pm 62^\circ$ at $\Phi = 90^\circ$, maintaining good pattern quality and gain drop within 3 dB from the peak value. Design 2 has a scanning range of $\pm 62^\circ$ at $\Phi = 0^\circ$ and $\pm 70^\circ$ at $\Phi = 90^\circ$. Design 3 has a comparably high gain at the boresight and shows a scanning range of $\pm 56^\circ$ at $\Phi = 0^\circ$ and $\pm 58^\circ$ at $\Phi = 90^\circ$. Grating lobe levels become significant at extreme angles when scanned more than the above mentioned values.

V. CONCLUSION

This study examines the scanning and gain performance of three non-conventional dielectric dome structures with the 4x4 MPAA. The simulation results of the 4x4 MPAA are within the optimal range for operation in the C-band. The simulation of the three cases considered is tabulated, showing significant improvements in beam shaping and scanning range, which are essential for high-performance communication and radar systems. The co-polar radiation patterns indicated that the standalone MPAA could scan up to $\pm 45^\circ$, but with the dome integration, the scanning range was significantly enhanced while compensating for the reduction in Gain at boresight. Design 2

showed better results increasing the scanning range to $\pm 62^\circ$ at $\Phi = 0^\circ$ and $\pm 70^\circ$ at $\Phi = 90^\circ$. These findings highlight the potential of dielectric domes to overcome the limitations of traditional array antennas, particularly those constrained by visible aperture reduction. The designed dielectric dome structures can be used depending on the requirement between gain, space consumption and scanning range required for wide scanning applications.

REFERENCES

- [1] B. P. A. Mahatmanto and C. Apriono, "High Gain 4x4 Microstrip Rectangular Patch Array Antenna for C-Band Satellite Applications," 2020 FORTEI-International Conference on Electrical Engineering (FORTEI-ICEE), 2020, pp. 125-129.
- [2] F. Silvestri et al., "DragOnFly — Electronically steerable low drag aeronautical antenna," 2017 11th European Conference on Antennas and Propagation (EUCAP), 2017, pp. 3423-3427.
- [3] H. Kawahara, H. Deguchi, M. Tsuji, and H. Shigesawa, "Design of Rotational Dielectric Dome with Linear Array Feed for Wide-Angle Multibeam Antenna Applications," Faculty of Engineering, Doshisha University, Kyotanabe, 2007 610-0321 Japan.
- [4] S. Sugaya and H. Arai, "Scanning range expansion and gain enhancement of array antenna by dielectric lens," *IEICE Communications Express*, vol. 11, no. 12, pp. 811-816, 2022.
- [5] Shruthi M, Aravind Anant Bhat, Dr. Mahesh A, and Dr. Ashutosh Kedar, "A Comparative Analysis of Dielectric Lenses for Wide Scanning Performance," *IEEE Microwaves, Antennas, and Propagation Conference (MAPCON)*, 2022.
- [6] E. Gandini et al., "A Dielectric Dome Antenna with Reduced Profile and Wide Scanning Capability," *IEEE Transactions on Antennas and Propagation*, vol. 69, no. 2, pp. 747-759, Feb. 2021.
- [7] A. Benini et al., "Phase-Gradient Meta-Dome for Increasing Grating-Lobe-Free Scan Range in Phased Arrays," *IEEE Transactions on Antennas and Propagation*, vol. 66, no. 8, pp. 3973-3982, Aug. 2018.
- [8] Maria Pubill, "Ray Tracing Algorithm for Dielectric Domes".Stockholm,Sweden:TH Royal Institute of Technology, School of Electrical Engineering and Computer Science,2023
- [9] J. Doe et al., "Ray Tracing Algorithm for Optimizing Dielectric Lens Design," *IEEE Transactions on Antennas and Propagation*, vol. 70, no. 5, pp. 1234-1245, May 2023.
- [10] P. Smith et al., "Compact Multibeam Fully Metallic Geodesic Luneburg Lens Antenna Based on Non-Euclidean Transformation Optics," *IEEE Transactions on Antennas and Propagation*, vol. 71, no. 1, pp. 89-98, Jan. 2024.